Interfaces within strain gradient plasticity

Aifantis, K.E.; Soer, W.A.; de Hosson, J.T.M.; Willis, J.R.

Published in:
Acta Materialia

DOI:
10.1016/j.actamat.2006.06.040

Publication date:
2006

Available online at www.sciencedirect.com
ScienceDirect
Acta Materialia 54 (2006) 5077–5085
Acta MATERIALIA
www.actamat-journals.com

Interfaces within strain gradient plasticity: Theory and experiments

K.E. Aifantis [a,b], W.A. Soer [a], J.Th.M. De Hosson [a,*], J.R. Willis [b]

[a] *Department of Applied Physics, Netherlands Institute for Metals Research and Materials Science Center, University of Groningen, Nijenborgh 4, 9747 AG Groningen, The Netherlands*

[b] *Department of Applied Mathematics and Theoretical Physics, Centre for Mathematical Sciences, University of Cambridge, Wilberforce Road, Cambridge CB3 0WA, UK*

Received 2 April 2006; accepted 23 June 2006
Available online 14 September 2006

Abstract

In this paper, it is shown that the occurrence of dislocation pileups across grain boundaries, as well as subsequent emission to the adjacent grains, is captured theoretically by gradient plasticity and confirmed experimentally by nanoindentation. From a theoretical point of view, this is accomplished (within a deformation theory framework applicable to continued loading) by accounting for a specific interfacial term in the overall potential of the material, in terms of which its response, taken to conform to strain gradient plasticity, is defined. The main features that result from the addition of this interfacial term are (i) significant size effects of Hall–Petch type in the overall stress–strain response of polycrystals and (ii) the determination of an analytical expression for the stress corresponding to the onset of dislocation transfer across interfaces. From an experimental point of view, the effective stress at which dislocation transfer takes place across an interface can be obtained from nanoindentations performed in close proximity to an Fe–2.2 wt.% Si grain boundary, since they exhibit a distinct strain burst that is related to the presence of the boundary. It is possible, therefore, to fit the theoretically determined analytical expression for the interfacial yield stress to the experimental data. From this fit, first estimates are obtained for key material parameters, namely the interfacial term and the internal length, that are required for the theoretical formulation. Dislocation mechanics are employed to provide physical insight of these parameters.

Keywords: Grain boundary; Dislocations; Plasticity; Nanoindentation; Fe–Si bicrystal

1. Introduction

The advent of a robust gradient plasticity theory [1,2] allowed for the determination of the widths and spacings of shear bands, described dislocation patterning and dispensed with the mesh dependence of finite element calculations in the material softening regime. Other interesting deformation phenomena such as interfaces, size effects and elimination of dislocation singularities [3,4] have been captured and other types of strain-gradient plasticity theories have been proposed. Among those developed during the past decade one distinguishes the works of Fleck and Hutchinson and co-workers [5–7] who developed a Cosserat-type strain-gradient plasticity and applied it for interpreting plasticity at the micrometer scale, including size effects. More recently, this theory has been revised [8] to remove certain deficiencies related to the elastoplastic coupling within the higher order gradient setting and incorporated in it the advantages of the Aifantis formulation [1,2], thereby rendering the theory more efficient computationally. A mathematically more appealing formulation of a deformation-type gradient plasticity theory was recently provided and applied, in conjunction with appropriate boundary and continuity (across interfaces) conditions, to derive effective properties of composites [9].

The formulation [9], however, has a significant limitation: size effects are limited by the Voigt upper bound. This is not intrinsic to the gradient theory, but results from the continuity conditions that were assumed across internal

* Corresponding author.
E-mail address: j.t.m.de.hosson@rug.nl (J.Th.M. De Hosson).

1359-6454/$30.00
doi:10.1016/j.actamat.2006.06.040

surfaces. It is possible, however, to treat interfaces as surfaces of discontinuity for the plastic strain gradient. The physical rationale behind this assumption is that dislocations pileup on interfaces, resulting in enhanced plastic strain gradients near interfaces. Therefore, Aifantis and Willis added into the overall energy functional that describes the material's response an interfacial potential term [10,11], which depends on the plastic strain on the interface and penalizes the buildup of plastic strain there. This allowed significant size effects to be obtained that were not limited by an upper bound, and which in the case of one-dimensional examples were solely due to the presence of this interfacial penalty. A distinctive feature of this formulation is that interfaces can follow their own yield behavior and, depending on the form of the interfacial penalty, an interfacial yield-like condition can be developed as well as a corresponding "interfacial yield" stress, which indicates the stress at which dislocations begin crossing the interface. It should be noted here that Gudmundson [12] recognized that gradient plasticity permitted the admission of new jump conditions across interfaces but made no detailed development like that contained in the present work and in Ref. [10].

The aforementioned "interfacial yield" stress can be related to the dislocation transference phenomenon that has recently been observed with nanoindentation near grain boundaries of body-centered cubic (bcc) metals [13–15]. During nanoindentation, the load required for the indenter tip to be displaced into the sample is recorded. In the commonly used load-controlled indentation mode, it has been observed that the load can remain constant while the tip is being displaced further into the surface. Such plateaus in the load vs. tip displacement plots are known as displacement or strain bursts and are related to dislocation motion; they have therefore been argued to indicate material yielding and/or fracture of surface oxides [16,17].

The purpose of the present article is to obtain first estimates of the parameters contained in the formulation put forward in refs. [10,11], from the nanoindentation experimental data. Therefore, after summarizing the formulation it is applied to a one-dimensional polycrystal and considered in relation to the experimental data. The formulation is first summarized (in Section 2) and then applied (in Section 3) to a simple one-dimensional example of a polycrystal. The analysis is straightforward and yields a simple explicit formula for the level of stress at which interfacial yielding begins. The experimental observations are summarized and compared with the theory in Section 4. The concluding Section 5 presents a brief summary and discussion.

2. Gradient plasticity with interfacial effects

In the theoretical formulations provided in Refs. [10,11], the form of the potential "energy" functional $\Psi(\varepsilon_{ij}, \varepsilon^P_{ij})$ of a gradient continuum was generalized to allow for the effect of internal boundaries (collectively denoted by Γ) by introducing an interfacial potential $\phi(\varepsilon^P_{ij})$.

This generalized expression for $\Psi(\varepsilon_{ij}, \varepsilon^P_{ij})$ reads

$$\Psi(\varepsilon_{ij}, \varepsilon^P_{ij}) = \int_\Omega U(\varepsilon_{ij}, \varepsilon^P_{ij}, \varepsilon^P_{ij,k})\mathrm{d}x + \int_\Gamma \phi(\varepsilon^P_{ij})\mathrm{d}\Gamma - \int_{S_T} (T^o_i u_i + t^o_{ij}\varepsilon^P_{ij})\mathrm{d}S, \tag{1a}$$

where Ω denotes the composite domain under consideration, and S_T is a part of the outer boundary $\partial\Omega$ over which tractions T^o_i, t^o_{ij}, conjugate to u_i, ε^P_{ij}, are prescribed. Both the displacement u_i and the plastic strain ε^P_{ij} are taken to be continuous throughout the whole domain under consideration. The total strain ε_{ij} is related to u_i through the usual expression $\varepsilon_{ij} = (u_{i,j} + u_{j,i})/2$. It should be noted that u_i, ε^P_{ij} are prescribed over the complementary part of the boundary $S_U = \partial\Omega - S_T$. The elastoplastic potential $U(\varepsilon_{ij}, \varepsilon^P_{ij}, \varepsilon^P_{ij,k})$ in Eq. (1a) is defined as

$$U(\varepsilon_{ij}, \varepsilon^P_{ij}, \varepsilon^P_{ij,k}) \equiv \frac{1}{2}L_{ijkl}(\varepsilon_{ij} - \varepsilon^P_{ij})(\varepsilon_{kl} - \varepsilon^P_{kl}) + V(\varepsilon^P_{ij}, \varepsilon^P_{ij,k}). \tag{1b}$$

It can be seen that the strain gradient comes in the plastic potential V.

Variables conjugate to the total strain; plastic strain and plastic strain gradient are defined as

$$\sigma_{ij} = \frac{\partial U}{\partial \varepsilon_{ij}} = L_{ijkl}(\varepsilon_{kl} - \varepsilon^p_{kl}), \tag{2a}$$

$$s_{ij} = \frac{\partial U}{\partial \varepsilon^p_{ij}} = -L_{ijkl}(\varepsilon_{kl} - \varepsilon^p_{kl}) + \frac{\partial V}{\partial \varepsilon^p_{ij}} = -\sigma_{ij} + \frac{\partial V}{\partial \varepsilon^p_{ij}}, \tag{2b}$$

$$\tau_{ijk} = \frac{\partial U}{\partial \varepsilon^p_{ij,k}} = \frac{\partial V}{\partial \varepsilon^p_{ij,k}}. \tag{2c}$$

It should be noted that Eq. (2c) defines the higher-order stress or hyperstress and results from use of the plastic strain-gradient as an internal variable.

Setting to zero the first variation of $\Psi(\varepsilon_{ij}, \varepsilon^p_{ij})$ ($\delta\Psi = 0$), we derive with the aid of Eqs. (1) and (2) the following principle of virtual work for a gradient continuum with internal boundaries:

$$\begin{aligned}
&\int_\Omega (\sigma_{ij}\delta\varepsilon_{ij} + s_{ij}\delta\varepsilon^p_{ij} + \tau_{ijk}\delta\varepsilon^p_{ij,k})\mathrm{d}x + \int_\Gamma \phi'(\varepsilon^p_{ij})\delta\varepsilon^p_{ij}\mathrm{d}\Gamma \\
&\quad = \int_{S_T} (T^o_i\delta u_i + t^o_{ij}\delta\varepsilon^P_{ij})\mathrm{d}S \\
&\quad \Rightarrow \int_\Omega (-\sigma_{ij,j}\delta u_i + (s_{ij} - \tau_{ijk,k})\delta\varepsilon^P_{ij})\mathrm{d}x \\
&\qquad + \int_{S_T} \{(\sigma_{ij}n_j - T^o_i)\delta u_i + (\tau_{ijk}n_k - t^o_{ij})\delta\varepsilon^P_{ij}\}\mathrm{d}S \\
&\qquad - \int_\Gamma ([\sigma_{ij}n_j]\delta u_j + ([\tau_{ijk}n_k] - \phi'(\varepsilon^P_{ij}))\delta\varepsilon^P_{ij})\mathrm{d}\Gamma = 0.
\end{aligned} \tag{3}$$

From Eq. (3), we obtain the following field equations:

$$\begin{aligned}
&\sigma_{ij,j} = 0, \\
&s_{ij} - \tau_{ijk,k} = 0 \quad \text{in } \Omega \setminus \Gamma
\end{aligned} \tag{4}$$

the boundary conditions

$$\sigma_{ij} = T_i^o, \quad \tau_{ijk} = t_{ij}^o \quad \text{on } S_T \tag{5}$$

and the jump conditions across interfaces

$$[\sigma_{ij} n_j] = 0, \quad [\tau_{ijk} n_k] = (\partial\phi/\partial\varepsilon_{ij}^p) \equiv \phi'(\varepsilon_{ij}^p) \quad \text{across } \Gamma. \tag{6}$$

The distinctive feature of this formulation is condition Eq. (6), since it provides the discontinuity for the higher order traction. The quantities in the brackets denote the jump from "side 1" to "side 2" across a point on the interface; while n_i points in the direction from "side 2" to "side 1."

Alternatively, if the displacements were taken to be prescribed on the outer boundary S_U, Eq. (5) would be replaced by

$$u_i = u_i^o, \quad \tau_{ijk} n_k = 0. \tag{7}$$

3. Application to a one-dimensional example

Explicit solutions will now be obtained for a simple one-dimensional model of a bicrystal. The specimen is taken to occupy the domain Ω which, in this case, is $-L < x < L$. The material is taken to be uniform, linearly hardening elastoplastic but it contains an interface (grain boundary) at $x = 0$. A distribution of strain $\varepsilon(x)$ with mean value $\bar{\varepsilon}$ is set up by the application of boundary displacements $u(-L) = -L\bar{\varepsilon}$, $(L) = L\bar{\varepsilon}$.

Symmetry implies that $\varepsilon(x)$ is an even function and hence it is necessary only to consider the region $0 < x < L$, with the boundary conditions

$$[\tau] \equiv 2\tau(0^+) = \phi'(\varepsilon^P)|_{x=0}; \tau(L) = 0, \tag{8}$$

in combination with the displacement conditions $u(0) = 0$, $u(L) = L\bar{\varepsilon}$ and the field equations in Eq. (4).

The assumed linear hardening is provided by the potential

$$V(\varepsilon^P, \varepsilon_x^P) = \sigma_0|\varepsilon^P| + \frac{1}{2}\beta[(\varepsilon^P)^2 + \ell^2(\varepsilon_x^P)^2]. \tag{9}$$

The constitutive relation, Eq. (2b), requires the term $\sigma_0|\varepsilon^P|$ to be interpreted as the limit of a smooth function; the result is that no plastic deformation is possible until the stress σ exceeds σ_0 in magnitude; β is a parameter that governs the hardening and ℓ is an internal length, which is also viewed as a material constant under the present formulation; the combined parameter $\beta\ell^2$ controls the flow stress enhancement provided by the plastic strain gradient. It can be seen that this form of V leads to the classical model of linear hardening (after yielding of the material) in the case that the gradient term, which contains the internal length ℓ, is neglected ($\ell \equiv 0$). Moreover, the strain-gradient contribution to hardening is taken to be similar in form to that of usual strain hardening.

The description is not complete until the interfacial potential $\phi(\varepsilon^P)$ is specified. This will be done soon but first relations for general ϕ are developed. Eq. (4) is satisfied by taking $\sigma = \bar{\sigma} =$ constant. Prior to grain interior yielding, i.e., $\varepsilon^P = 0$, Eq. (9) in combination with the appropriate limiting form of Eq. (2b) gives $|\bar{\sigma}| \leqslant \sigma_0$, while Eq. (2a), with the relevant elastic modulus denoted by E, reduces to $\bar{\sigma} = E\varepsilon$. Thus, the strain is constant and so equal to the specified mean strain $\bar{\varepsilon}$. This solution is valid so long as $|\bar{\varepsilon}| \leqslant \sigma_0/E$. Now suppose that $\bar{\varepsilon} > \sigma_0/E$. It is necessary to accept that $\varepsilon^P(x) > 0$, in which case Eqs. (9) and (2b, 2c) give

$$\varepsilon^P - \ell^2\varepsilon_{xx}^P = \frac{\bar{\sigma} - \sigma_0}{\beta}, \tag{10}$$

whose solution, allowing for the second boundary condition in Eq. (8), is

$$\varepsilon^P(x) = \frac{\bar{\sigma} - \sigma_0}{\beta} - A\cosh[(L - x)/l], \tag{11}$$

where A is a constant to be determined. The mean plastic strain follows as

$$\bar{\varepsilon}^P = \frac{\bar{\sigma} - \sigma_0}{\beta} - A(\ell/L)\sinh(L/\ell). \tag{12}$$

The constant A is fixed from the first of the boundary conditions in Eq. (8).

3.1. Linearly hardening interfacial potential

Now assume that the interface behaves similarly as the grain interior. Thus, in analogy with Eq. (9), the interfacial potential is taken to be

$$\phi(\varepsilon_0^P) = \gamma|\varepsilon_0^P| + \frac{1}{2}\alpha(\varepsilon_0^P)^2, \tag{13}$$

where $\varepsilon_0^P = \varepsilon^P(0)$ and γ and α are constants. It follows that γ is qualitatively similar to σ_0; in particular it can be considered as an interfacial tension term. In our description, the interfacial tension is numerically identical to the interfacial energy because the interfacial tension is independent of the interfacial area. From a physics viewpoint the interfacial energy is generally not numerically equal to the interfacial tension. However, this reservation is not important if the interface is atomically disordered or if the boundary between two phases is not of a special type (special Σ coincident site lattice boundaries) as in our bicrystal. Similar to β, α governs the hardening of the interface that results from the ongoing dislocation transference. The appropriate limiting form of the jump condition of the higher-order traction Eq. (6) results in the following "interfacial" yield-like condition:

$$[\tau]\begin{cases} \in [-\gamma, \gamma] & \text{if } \varepsilon_0^P = 0, \\ = \gamma\varepsilon_0^P/|\varepsilon_0^P| + \alpha\varepsilon_0^P & \text{otherwise.} \end{cases} \tag{14}$$

It is assumed throughout that the mean strain $\bar{\varepsilon}$ is positive. If $\bar{\varepsilon} \leqslant \sigma_0/E$, the plastic strain is zero and the mean stress is related to the mean strain by $\bar{\sigma} = E\bar{\varepsilon}$.

Suppose next that $\sigma_0/E < \bar{\varepsilon} \leqslant \bar{\varepsilon}_c$, where $\bar{\varepsilon}_c$ is the greatest strain for which the plastic strain ε_0^P at the interface remains zero (it will be determined below). Therefore, in this regime the constant of integration A is determined by setting the plastic strain, Eq. (12), on the interface equal to zero:

$$A = \frac{\bar{\sigma} - \sigma_0}{\beta}\operatorname{sech}(L/\ell). \tag{15}$$

Furthermore,

$$[\tau] = 2\beta\ell^2\varepsilon_x^P(0) = 2(\bar{\sigma} - \sigma_0)\ell\tanh(L/\ell) \tag{16}$$

and hence this solution is valid (assuming $\bar{\varepsilon} > 0$) so long as $\sigma_0 \leqslant \bar{\sigma} \leqslant \bar{\sigma}_c$, where

$$\bar{\sigma}_c = \sigma_0 + \frac{\gamma}{2l}\coth(L/\ell). \tag{17}$$

This solution is valid (assuming $\bar{\varepsilon} > 0$) so long as Eq. (16) is compatible with Eq. (14), with $\varepsilon_0^P = 0$; that is, so long as $\sigma_0 \leqslant \bar{\sigma} \leqslant \bar{\sigma}_c$.

Also, Eqs. (12) and (15) give

$$\bar{\varepsilon}^P = \frac{\bar{\sigma} - \sigma_0}{\beta^{\text{eff}}}, \tag{18}$$

where

$$\beta^{\text{eff}} = \beta[1 - (\ell/L)\tanh(L/\ell)]^{-1}. \tag{19}$$

Eq. (18) together with $\bar{\sigma} = E(\bar{\varepsilon} - \bar{\varepsilon}^P)$, which was obtained by averaging Eq. (2a), gives the mean stress–mean strain relation in this regime:

$$\begin{aligned}\bar{\sigma} &= \sigma_0 + \frac{\beta^{\text{eff}}}{1 + \beta^{\text{eff}}/E}(\bar{\varepsilon} - \sigma_0/E)\\ &= \sigma_0 + \frac{\beta}{1 + \beta/E - (\ell/L)\tanh(L/\ell)}(\bar{\varepsilon} - \sigma_0/E).\end{aligned} \tag{20}$$

The critical strain $\bar{\varepsilon}_c$ corresponds to the critical stress $\bar{\sigma}_c$ and can be obtained by combining Eq. (17) with Eq. (20). The result is

$$\bar{\varepsilon}_c = \frac{\sigma_0}{E} + \left(\frac{\gamma}{2\beta\ell}\right)\left[\left(1 + \frac{\beta}{E}\right)\coth(L/\ell) - \frac{\ell}{L}\right]. \tag{21}$$

Finally, consider the range of mean strain $\bar{\varepsilon} > \bar{\varepsilon}_c$, so that $\varepsilon_0^P > 0$. The boundary condition Eq. (8) implies that

$$A = \left(\frac{\gamma + (\alpha/\beta)(\bar{\sigma} - \sigma_0)}{\alpha\cosh(L/\ell) + 2\beta\ell\sinh(L/\ell)}\right) \tag{22}$$

and hence, from Eq. (12)

$$\bar{\varepsilon}^P = \frac{\bar{\sigma} - \sigma_0}{\beta} - \frac{[\gamma + (\alpha/\beta)(\bar{\sigma} - \sigma_0)](\ell/L)}{\alpha\coth(L/\ell) + 2\beta\ell}. \tag{23}$$

The relation between mean stress and mean strain can be obtained by combining Eq. (23) with $\bar{\varepsilon}^P = \bar{\varepsilon} - \bar{\sigma}/E$. The result can be expressed in the form

$$\bar{\sigma} - \sigma_c = \beta\left\{1 + \frac{\beta}{E} - \frac{[\alpha/(2\beta\ell)](\ell/L)}{1 + [\alpha/(2\beta\ell)]\coth([L/\ell)}\right\}^{-1}(\bar{\varepsilon} - \bar{\varepsilon}_c). \tag{24}$$

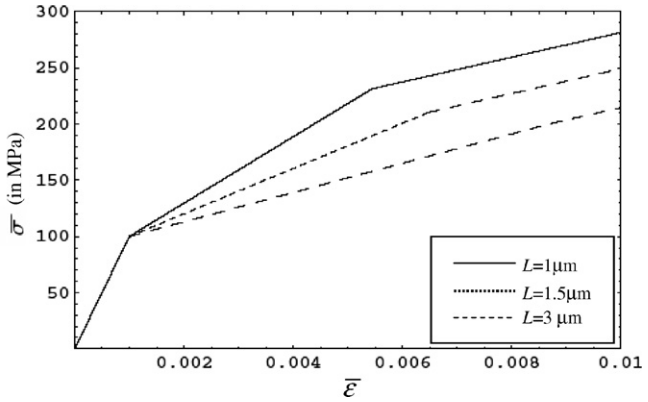

Fig. 1. Overall stress–strain relation (Eq. (25)) and size effects for a single-phase bicrystal; the first "knee" indicates grain interior yielding, while the second one "yielding" of the interface. The material parameters are given as $E = 100$ GPa, $\sigma_0 = 100$ MPa, $\beta = 10$ GPa, $\ell = 1$ μm, $\gamma = 200$ N/m, $\alpha = 10$ N/m.

Thus, the complete mean stress–mean strain relation for this medium is

$$\bar{\sigma} = \begin{cases} E\bar{\varepsilon}, & 0 \leqslant \bar{\varepsilon} \leqslant \sigma_0/E,\\ \sigma_0 + \frac{\beta}{1+\beta/E-(\ell/L)\tanh(L/\ell)}(\bar{\varepsilon} - \sigma_0/E), & \sigma_0/E \leqslant \bar{\varepsilon} \leqslant \bar{\varepsilon}_c,\\ \sigma_c + \beta\left\{1 + \frac{\beta}{E} - \frac{[\alpha/(2\beta\ell)](\ell/L)}{1+[\alpha/(2\beta\ell)]\coth(L/\ell)}\right\}^{-1} & (\bar{\varepsilon} - \bar{\varepsilon}_c),\ \bar{\varepsilon}_c \leqslant \bar{\varepsilon}. \end{cases} \tag{25}$$

Eq. (25) is plotted in Fig. 1 with the values $E = 100$ GPa, $\sigma_0 = 100$ MPa, $\beta = 10$ GPa, $\ell = 1$ μm, $\gamma = 200$ N/m, $\alpha = 10$ N/m for a range of values of L. The first portion of these curves indicates the purely elastic response of the material according to Eq. (25). After yielding of the grain interior, which is indicated by the first "knee" in the plots, two physical mechanisms occur. Initially, the interface remains impermeable to dislocations, leading to a stiffening mechanism. This "stiffening" mechanism enhances the linear hardening taking place in the grain interior and the overall response is depicted in the second linear segment of Fig. 1. After the applied stress reaches a critical value ($\bar{\sigma}_c$), causing yielding of the interface (second "knee") and allowing dislocations to penetrate it, both the grain boundary and the grain interior deform in a linear hardening manner. It can be seen that Fig. 1 exhibits Hall–Petch-type scale effects since as the grain size L decreases the stress required for continuous plastic deformation increases. It should be noted here that the prediction of size effects results from consideration of strain gradients, and since no allowance for elastic strain gradients was made no size effects were observed in the purely elastic region (first linear segment) of Fig. 1.

4. Relating gradient plasticity to nanoindentation data

The previous section demonstrated that gradient plasticity allows interfaces to follow their own yield behavior and hence an "interfacial yield" stress, Eq. (17), is present; in particular this stress increases in inverse proportion to

the grain size. It is independent of the hardening parameter β and is thus essentially a property of the interface. The purpose of this section is to confirm through experimental observations the existence of such an "interfacial yield" stress, as well as the occurrence of corresponding size effects.

The possibility of measuring an intrinsic hardening contribution of the grain boundary, as a result of the difficulty in slip transmission across the boundary, has recently come under investigation with the widespread availability of the nanoindentation technique. Such experiments could potentially offer detailed information about the intrinsic mechanical properties of individual grain boundaries. So far, however, a thorough understanding of the mechanical response is lacking.

Recent studies [14,15] have shown that nanoindentation measurements in the direct proximity of grain boundaries in bcc metals show typical yield excursions, i.e., plateaus in the load vs. penetration depth nanoindentation plots. Based on the indentation load and depth at which these excursions are observed, it was proposed that they are strain bursts due to dislocation pileup and subsequent transmission across the boundary. In the following, the relevant experimental procedures are summarized, and indentation results for an Fe–2.2% Si bicrystal are presented and related to the aforementioned gradient plasticity approach.

A bicrystalline specimen of an Fe–2.2% Si alloy prepared by floating-zone melting was used for the indentation experiments. The misorientation of the grain boundary is represented by a [−0.290.120.03] Rodrigues vector and does not correspond to a low-index coincident site lattice. The Fe–2.2% Si specimen contained traces of phosphorus and carbon [18]. The specimen surface was polished using a final polishing colloidal silica suspension. Electron backscatter diffraction (EBSD) was employed to locate the grain boundary with respect to a grid of marker indents.

Nanoindentation measurements were carried out employing an MTS Nano Indenter XP (MTS Nano Instruments, Oak Ridge, TN) with a pyramidal Berkovich tip using the continuous stiffness measurement (CSM) technique. Load-controlled indentations were made to a maximum depth of 200 nm with a targeted strain rate of 0.05/s, which corresponds to a maximum loading rate of the order of 0.1 mN/s. The azimuthal orientation of the indenter was chosen to have one side of the triangular impression of the Berkovich tip parallel to the grain boundary under investigation. In order to vary the distance to the boundary with the smallest possible increments, lines of indentations were drawn across the grain boundary at angles smaller than 3° with a spacing of 3 μm between the indents. Although the plastically deformed zones of consecutive indents are likely to overlap at such close spacing, no significant effect of any cross-talk interaction on the measured response was found in a test comparing lines of indents of 200 nm depth with spacings ranging from 3 to 10 μm in the Fe–2.2% Si matrix.

Three lines of 60 indentations crossing the grain boundary were performed on one polished surface of the specimen, and another line was performed on the same surface after repolishing. The experiment was therefore repeated four times in total. All indentations exhibited a plateau (in the load vs. depth plot) at a constant load of around 50 μN as illustrated by (A) in Fig. 2(a); this plateau is indicative of grain interior yielding (Fig. 2(a)). For some indentations that were in close proximity to the boundary (i.e., when the distance from the center of the indent to the boundary was less than 1 μm) a second plateau was observed well beyond the first one. It is believed that such displacement bursts near grain boundaries indicate the onset of dislocation motion across them, or the activation of dislocation sources in the adjacent grain; this is similar to what is termed interfacial yielding in the aforementioned gradient plasticity theory. The occurrence of two subsequent strain bursts, i.e., after initial grain interior yielding, may indicate that dislocation transference proceeds by dislocation absorption into the boundary and subsequent dislocation emission in the adjacent crystal as put forward in Ref. [15]. In this respect, it is relevant to point out that these strain bursts correspond to a decrease in hardness, i.e., once the strain bursts were reached the hardness decreased, implying that the stress on the boundary is relieved though dislocation transfer or activation of dislocation sources in

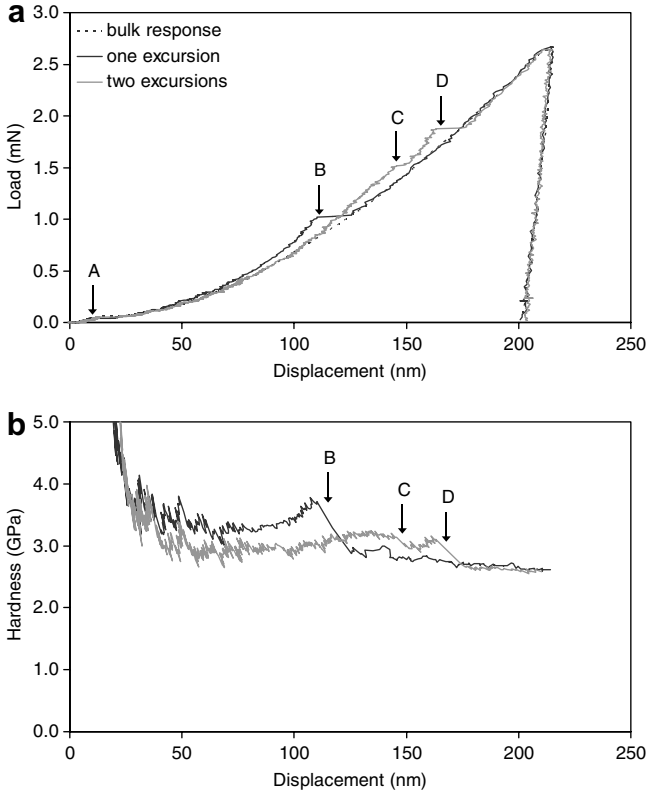

Fig. 2. (a) Load vs. displacement curves obtained from the grain interior (dashed line) and near the grain boundary (solid lines). All indentations show an initial yield point at a load around 50 μN (A). Either one (B) or two (C and D) characteristic strain bursts are observed for indentations near the grain boundary at substantially higher loads. (b) CSM hardness profiles corresponding to the loading curves shown in (a).

the adjacent grain (Fig. 2(b)). Since the nanoindentation experiments were performed using the CSM method, hardness vs. depth plots could be constructed from the recorded phase angle. Therefore, the hardness at the onset of the aforementioned strain bursts could be obtained; see Table 1.

Since the aforementioned theory makes use of stress, not hardness, the crystallography of the specimen is employed in order to obtain estimates for the grain boundary yield stress. We assume a uniaxial compressive stress perpendicular to the surface of the indenter and use Schmid behavior as a first approximation. Since the indentation hardness by definition is equal to the applied average stress, the applied resolved shear stress τ_a can be calculated from EBSD analyses. We found that the Schmid factor is close to 0.5 as further detailed in Ref. [14]. The resolved shear stress may therefore be approximated at any time during the indentation as half of the measured hardness, $\tau_a = H/2$.

It should be mentioned here that prior indentation studies [19,20] have also shown an increase in hardness as the grain boundary was approached. This hardening, however, was attributed to segregation of impurities on grain boundaries, and not to the fact that the boundary opposed dislocation motion. This was concluded from the fact that indentations right on the boundary gave the highest hardness (due to the impurities they contained), even though there was nothing limiting dislocation motion on either side. In the present experimental data, however, different behavior is observed. As the grain boundary is approached the hardness increases significantly; however, once the indenter tip hits the boundary, the hardness drops to values observed in the grain interior. This suggests that the increase in hardness near the grain boundary is not due to segregation, but due to dislocation pileups that result from the presence of the boundary (see also Fig. 5 in Ref. [15]).

Although most of these indents crossed over the boundary at maximum indentation depth, see Table 1, it is readily concluded from the load–displacement data that the indenter was still well away from the boundary at the instant of the excursion, at distances ranging from 0.11 to 0.34 μm. It should be emphasized that this behavior was not found for any of the indentations in the matrix, but also not all indents crossing the boundary displayed such a burst.

In six of the nine indentations, the material yielded, i.e., after initial grain interior yielding, in one displacement burst at constant load, as shown in Table 1; the other three curves show two distinct bursts, which are separated by a loading portion. In fact, in the experiments two indentations (i.e., with depth of onset of burst 135 and 146 nm, respectively) exhibited a slightly increasing load during the burst instead of a perfect horizontal plateau, e.g., see curve C in Fig. 2(a). Nevertheless, the ascending curve is not treated here as a separate physical phenomenon. One should realize that in the load-controlled experiments, i.e., not displacement controlled, the burst is defined just by two points, one before and the other just after the burst (see Fig. 2(b)). The ascending curve is simply a slight increase of the load during a strain burst because of limitation of the feedback system. The strain bursts lead to very rapid changes in the contact stiffness and it may therefore be anticipated that the feedback system is not able to perfectly capture all these events at constant load. An even more important observation is that in all cases a burst was preceded with an increase in hardness indicating an increase in stored energy in front of the interface (Fig. 2(a)). When two distinct strain bursts were present, the first is considered to indicate grain boundary yielding.

Because different polishing procedures were followed one may wonder about modifications of the subsurface area and whether the corresponding data should be treated differently. Indeed, the density of dislocations will be affected by polishing and if the density is higher, the amount of dislocations in the pileup required to generate the critical shear stress will be reached earlier during the loading cycle. Nevertheless, the recorded hardness, which is directly related to this critical shear stress, will be effectively the same. Therefore, all the experimentally obtained

Table 1
Indentation data for observed yield excursions (bursts) at the boundary in the Fe–Si bicrystal; "1st" and "2nd" denote indentations that showed two separate bursts

Line	Indent	Initial distance to boundary	Distance to boundary at onset of burst	Load at onset of burst	Depth at onset of burst	Length of burst	CSM hardness before burst
		d_{center} (nm)	d_{burst} (nm)	P (mN)	h (nm)	Δh (nm)	H (GPa)
1	1	493	210	1.24	130	11	3.20
	2	370	131	1.02	110	16	3.70
2	1	665	335	1.67	152	10	3.17
	2	517 1st	223	1.39	135	4	3.33
		2nd	189	1.79	151	20	
3	1	597	169	2.83	197	19	3.20
	2	463 1st	146	1.52	146	4	3.17
		2nd	109	1.88	163	13	
	3	330 1st	106	1.01	103	6	4.25
		2nd	78	1.16	116	13	
1 (2nd surface)	1	740	310	2.58	198	9	2.68
	2	555	196	1.91	165	12	2.88

data are presented in Table 1. The last two indents listed in Table 1 were taken from a surface that was polished in a different way than the rest. Although there are no real physical arguments to delete these observations in the confrontation with the theoretical analysis we keep this in mind and present fits with and without the last two data points of Table 1.

In Section 3, an analytical expression, Eq. (17), was obtained for the "interfacial yield" stress of a single-phase bicrystal. In the further analysis, we do not account for a grain interior yield stress because the purely elastic region that was observed in the nanoindentations of the Fe–2.2% Si bicrystal is almost negligible. In fact, in Fig. 2, it is further illustrated that the purely elastic deformation experienced by the bicrystal at hand is very small, and it is therefore appropriate not to account for grain interior yielding. Based on the above discussion it is reasonable to fit the interfacial yield stress expression given by Eq. (17), with σ_0 set to zero, to the experimental data of Table 1. It should be noted that the indenter tip to grain boundary distance can be treated as the specimen size since it is bounded on both sides. It is seen in Fig. 3 that, even though Eq. (17) was derived under one-dimensional considerations, without explicitly considering the physics and mechanics that come into play during an indentation, it fits well the experimental data as shown by the solid line. This fit including all the data of Table 1 provides approximate values for the internal length $\ell = 120$ nm of Fe–2.2% Si, as well as for the interfacial energy-like term $\gamma = 349$ N/m associated with its grain boundary. If the last two data points are ignored because the experiments were done on differently polished surfaces the internal length ℓ becomes 107 nm and the interfacial energy-like term γ is 330 N/m (see also dashed line in Fig. 3). Indeed, the fit to all the data produces an internal length that is somewhat larger than the smallest specimen size, which is 106 nm (see Table 1). The fit including all the data are slightly off compared with a fit to the confined data set. Since these are the first estimates to be obtained for these parameters their validity will be assessed through dislocation mechanics considerations in the paragraphs to follow.

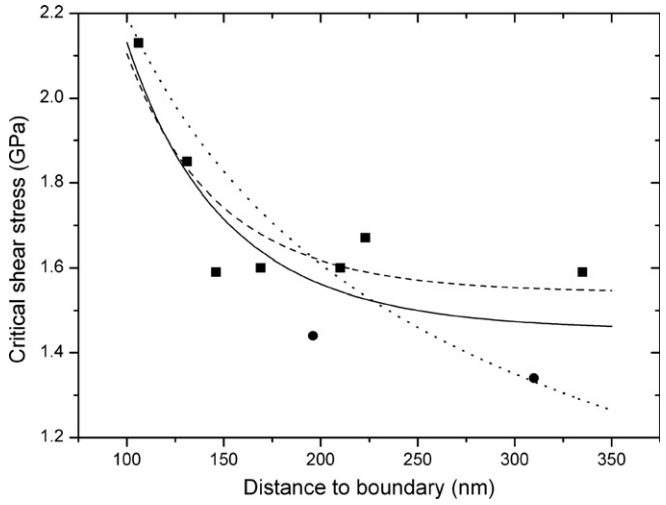

Fig. 3. Hall–Petch relation (dotted line) and analytical relation obtained through gradient plasticity fitted all to the experimental data points (solid line) and fitted to the data of only surface 1 (dashed line). Squares refer to surface 1 and dots to surface 2.

First, however, it is interesting to compare the interfacial yield stress expression to the fit obtained by the classic Hall–Petch relation as shown by the dotted line in Fig. 3. The approach that was followed to apply the Hall–Petch relation to this particular experimental situation has been described in detail in Refs. [14,15]. Both the analytical expression derived in this paper and the Hall–Petch relation clearly show the trend of increasing interfacial yield stress with decreasing distance to the boundary and provide a reasonable fit to the data points with R^2 values of 0.76 and 0.48, respectively. In the limit of large distances to the boundary, the functions converge to different values: the Hall–Petch relation converges to the intrinsic frictional shear stress $\tau_0 = 200$ MPa, while the gradient plasticity relation approaches $\gamma/2\ell = 1.45$ GPa. One source for this discrepancy is that the gradient plasticity relation is based on a formulation that assumes linear hardening, which is not allowed for in the classic Hall–Petch model. Another is the fact that the one-dimensional theory presents a better description of the experimental situation at small distances than it does at larger distances, where the three-dimensional properties of the setup become more relevant, e.g., through cross-slip of dislocations and the geometry of the indenter. Physically, the yield stress of the boundary in this limit has little meaning, since it cannot be measured at large distances from the boundary with the present indentation technique.

Since the dislocations initiate at the indenter tip and pileup at the boundary this distance can be thought of as the dislocation pileup length; furthermore the equilibrium pileup length can be taken to be the maximum indenter tip to grain boundary distance for which a distinct strain burst, indicating boundary yielding, was observed. This is so because in order to observe grain boundary yielding, dislocation pileups must first form. In particular, we have that

$$l_{\text{pile-up}} = \frac{\mu b n}{\pi \tau_a}, \tag{26}$$

where n is the number of dislocation loops in the pileup, ignoring the difference between edge and screw parts, b is the magnitude of the Burgers vector and τ_a is the applied shear stress. From Table 1 the distance from the indenter to the grain boundary at the onset of the burst is estimated to be of the order of 200 nm and we obtain an estimate for the pileup length and applied shear stress, being, respectively, $l_{\text{pileup}} = 200$ nm, and $\tau_a = 1.5$ GPa; moreover $b = 0.25$ nm, while the shear modulus of Fe–2.2% Si is taken from the indentation data to be 95 GPa. Inserting therefore these values in Eq. (26), it is estimated that the maximum number of dislocations that can extend from the grain boundary to the indenter tip is approximately

40. Plotting this dislocation distribution with respect to the pileup length suggests that 90% of the dislocations, which are responsible for plastic strain gradients, are positioned within 110 nm from the boundary (Fig. 4). This is consistent with the fit estimate for the internal length since the internal length denotes the characteristic length in which gradients of the plastic strain are most noticeable and hence size effects are observed. By comparing Eq. (17) with Eq. (26) it could be said that γ can be viewed as an effective modulus of the interface depending on the number n of dislocations with a Burgers vector b, which are distributed over a certain length scale, ℓ, in front of the interface.

Essential points for discussion of the linkage to the experimental data are the imposed symmetry and the dimensionality in the mathematical treatment of the problem. The indentation measurements on the Fe–Si bicrystal show a marked dependence on the azimuthal orientation of the indenter with respect to the boundary. Both the characteristic yield excursions and the increased hardness are observed only when one side of the indenter is facing the boundary. This was verified by an additional measurement with the indenter rotated 180° to eliminate the possibility that this observation is due to the crystallographic asymmetry across the boundary. The orientation dependence can be understood by approximating the stress field by uniaxial pressure components perpendicular to the faces of the indenter, and recognizing that the resolved shear stress at the grain boundary is a maximum when one side is facing the boundary. As a consequence the nanoindentation experiment can be considered as a uniaxial compression test. We consider here in particular grain boundary yielding and not the flow stress including hardening after yielding. In the latter case three-dimensional dislocation interactions like forest dislocation interactions and geometrically necessary dislocations come into play. Because of the limited volume between the indenter and the grain boundary the interactions between the dislocations and the grain boundary in the experiments are more or less one-dimensional. Indeed, in reality there is a two-dimensional effect of orienting the dislocation line to the specific grain boundary plane ($(1\,\bar{1}\,2)[\bar{1}\,1\,1]$ slip is transmitted to the $(\bar{1}\,0\,1)[1\,1\,1]$ system in the adjacent grain [14]) but for the grain boundary yielding problem considered this is of less importance. Although Eq. (17) applies strictly only to the one-dimensional symmetrical example for which it was derived, it is considered likely that its general form is representative of the stress that would be required in the vicinity of an interface to induce dislocation transmission, or nucleation at the interface, and hence plastic deformation at the interface. In that spirit, the simple formula is fitted to the results of the nanoindentation experiments, which were performed on a bicrystal in the vicinity of the grain boundary. Estimating the stress that would be required for a dislocation pileup generated by the indentation to "break through" the interface provides a "sanity check" on the values of the parameters that are obtained. There is, of course, significant uncertainty, concerning the applicability of the one-dimensional strain-gradient theory, and the essentially one-dimensional dislocation pileup analysis, to the nanoindentation experiment; estimation of the local stress in the experiment from measurement of the hardness is likely also to be subject to some error. In particular, we anticipate that the value from the fitting procedure for the interfacial energy-like term $\gamma = 349$ N/m associated with its grain boundary is rather high because of the one-dimensional theory vs. three-dimensional effects in experiments, whereas the value for the internal length ℓ will be less affected by this and bears therefore a better physical meaning. Subject to these caveats, however, the results of the present study are considered encouraging, and a necessary precursor to further pursuit of theory of this type, in the context of three-dimensional fields of deformation.

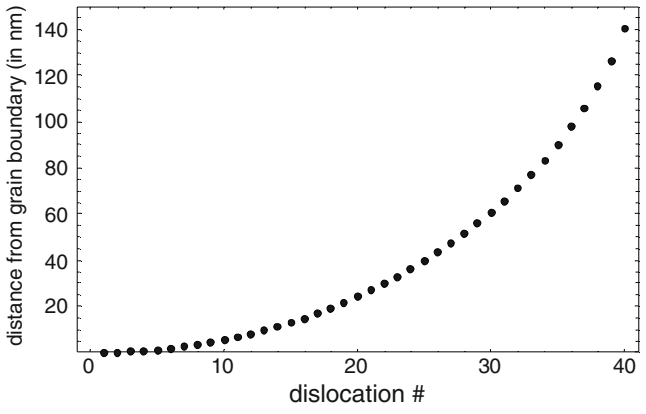

Fig. 4. Distribution of 40 dislocations under an applied shear stress of 1.5 GPa in front of the Fe–2.2% Si grain boundary.

5. Conclusions

Based on experimental evidence the purely elastic deformation experienced by an Fe–2.2% Si bicrystal during an indentation was almost negligible; the same experimental data suggest that indenting near the grain boundary results in dislocation pileups and subsequent emission to the adjacent grain. To model this behavior theoretically, a purely plastic gradient-dependent potential characterizing the response of a bicrystal, and a nonlinear potential characterizing the grain boundary behavior, were considered. Fitting the experimental data to the analytical expression obtained for the interfacial yield stress allows the determination of the material parameters that come into play in the theoretical formulation. It is predicted that the internal length (ℓ) and interface parameter (γ) for Fe–2.2% Si are of the order of 110 nm and 330 N/m, respectively. In fact, it is shown through dislocation mechanics, that this length scale in front of the grain boundary corresponds to a distance over which 90% of the dislocations are piled up; this result is in agreement with the internal length value obtained from the fit since ℓ denotes a characteristic material length over which gradients in the plastic strain are most significant.

Acknowledgements

The authors thank Pavel Lejcek and Tomas Vystavel for providing the bicrystal specimens. This work was funded by the Netherlands Institute for Metals Research under project number MC4.01104. K.E.A. is grateful to Professor Ali S. Argon for enlightening discussions and acknowledges the US National Science Foundation for its support through the Graduate Research Fellowship Program. K.E.A. is currently with the Department of Mechanics, St. Petersburg State University, Russia.

References

[1] Aifantis EC. J Eng Mater Technol 1984;106:326.
[2] Aifantis EC. Int J Plasticity 1987;3:211.
[3] Aifantis EC. Int J Eng Sci 1995;33:2161.
[4] Aifantis EC. Mech Mater 2003;35:259.
[5] Fleck NA, Hutchinson JW. J Mech Phys Solids 1993;41:1825.
[6] Fleck NA, Hutchinson JW. In: Hutchinson JW, Wu TY, editors. Adv Appl Mech, 33. New York (NY): Academic Press; 1997. p. 295.
[7] Fleck NA, Müller GM, Ashby MF, Hutchinson JW. Acta Metall Mater 1994;42:475.
[8] Fleck NA, Hutchinson JW. J Mech Phys Solids 2001;49:2245.
[9] Fleck NA, Willis JR. J Mech Phys Solids 2004;52:1855.
[10] Aifantis KE, Willis JR. In: Kounadis A, Providakis C, Exadaktylos G, editors. Proceedings of seventh national congress on mechanics, June 24–26, 2004, vol. II, Chania, Greece; 2004. p. 372.
[11] Aifantis KE, Willis JR. J Mech Phys Solids 2005;53:1047.
[12] Gudmunson PJ. J Mech Phys Solids 2004;52:1379.
[13] Wang MG, Ngan AWH. J Mater Res 2004;19:2478.
[14] Soer WA, De Hosson JTM. Mater Lett 2005;59:3192.
[15] Soer WA, Aifantis KE, De Hosson JTM. Acta Mater 2005;53:4665.
[16] Bahr DF, Kramer DE, Gerberich WW. Acta Mater 1998;46:3605.
[17] Corcoran SG, Colton RJ, Lilleodden ET, Gerberich WW. Phys Rev 1997;B55:16057.
[18] Lejcek P. Anal Chim Acta 1994;297:165.
[19] Aust KT, Hanneman RE, Niessen P, Westbrook JH. Acta Metall 1968;16:291.
[20] Watanabe T, Kitamura S, Karashima S. Acta Metall 1980;28:455.